

# Bulk-sensitive Photoemission of $\text{Mn}_5\text{Si}_3$

A. Irizawa<sup>a</sup>, A. Yamasaki<sup>a</sup>, M. Okazaki<sup>a</sup>, S. Kasai<sup>a</sup>,  
A. Sekiyama<sup>a</sup>, S. Imada<sup>a</sup>, S. Suga<sup>a</sup>, E. Kulatov<sup>b</sup>, H. Ohta<sup>c</sup>,  
T. Namba<sup>d</sup>

<sup>a</sup>*Graduate School of Engineering Science, Osaka University, Toyonaka, Osaka  
560-8531, Japan*

<sup>b</sup>*General Physics Institute, Russian Academy of Science, Moscow, Russia*

<sup>c</sup>*Molecular Photoscience Research Center, Kobe University, Rokkodai, Nada, Kobe  
657-8501, Japan*

<sup>d</sup>*The Graduate School of Science and Technology, Kobe University, Rokkodai,  
Nada, Kobe 657-8501, Japan*

---

## Abstract

We have carried out a bulk-sensitive high-resolution photoemission experiment on  $\text{Mn}_5\text{Si}_3$ . The measurements are performed for both core level and valence band states. The Mn core level spectra are deconvoluted into two components corresponding to different crystallographic sites. The asymmetry of each component is of noticeable magnitude. In contrast, the Si 2p spectrum shows a simple Lorentzian shape with low asymmetry. The peaks of the valence band spectrum correspond well to the peak positions predicted by the former band calculation.

*Key words:*  $\text{Mn}_5\text{Si}_3$ , Transition-metal silicide, Photoemission

*PACS:* 71.20.Lp, 75.20.En, 79.60.-i

---

## 1 Introduction

Transition metal silicide  $\text{Mn}_5\text{Si}_3$  has been known to show complex magnetic phase transitions [1,2,3,4,5]. Its crystal structure is  $D8_8$  and has two inequivalent crystallographic sites; namely, two Mn atoms in the 4(d) position ( $\text{Mn}_I$  4(d)), as well as three Mn atoms and three Si atoms in the 6(g) position ( $\text{Mn}_{II}$  6(g)) in the formula unit cell [6,7]. This compound shows the Curie-Weiss type paramagnetic state over 99 K, collinear antiferromagnetic state between 66 and 99 K, and non-collinear antiferromagnetic state below 66 K with a complex spin structure [4]. Below 66 K, it also shows a field-induced

magnetic transition which is attributed to its topological frustration of spin alignment in the non-collinear antiferromagnetic structure [1,2]. The electric resistivity represents a metallic behavior with two kinks corresponding to these phase transitions [1,5]. Some conceivable magnetic structures are proposed for the collinear and non-collinear magnetic phases from the neutron diffraction studies [8,9,10,11,12]. For the non-collinear phase at lower temperatures, for example, it is considered that several Mn sites with different magnitude and orientation of the magnetic moments are providing itinerant electrons. However, their electronic states are still unclear. Thus, measurements of core-level and valence band photoemission are very important to reveal their complex electronic states.

In this study, we have performed a bulk-sensitive high-resolution photoemission spectroscopy of  $\text{Mn}_5\text{Si}_3$  for the paramagnetic state.

## 2 Experimental

Single crystals of  $\text{Mn}_5\text{Si}_3$  were prepared by Czochralski method. Clean surfaces were obtained by scraping with a diamond file. Measurements were carried out at the beam line BL25SU in SPring-8 by using a SCIENTA-200 electron analyzer under the base pressure of better than  $5 \times 10^{-10}$  Torr. The excitation photon energy was set to 900 eV for the bulk-sensitive experiments. The total energy resolution was set to about 100 meV for the valence band region and about 200 meV for the core-level photoemission. These values are used for the analyses of spectral deconvolution as the Gaussian width as performed later. The measurements were done at 195 K at which  $\text{Mn}_5\text{Si}_3$  is in the Curie-Weiss type paramagnetic state with metallic conductivity [1,4].

## 3 Results and Discussion

Figures 1(a)-(d) show the core-level photoemission spectra of  $\text{Mn}_5\text{Si}_3$ . The Si 2p doublet ascribable to the  $j=3/2$  and  $1/2$  spin-orbit components is clearly observed as shown in Figure 1(a). The spectral shape can be fit by a single component for both  $j=3/2$  and  $1/2$  components by adopting the Doniach-Sunjic line shape [13]. The asymmetry parameter of  $\alpha=0.017$  is employed for both  $j=3/2$  and  $1/2$  peaks. The values of the experimental full width at half maximum (FWHM) are 0.43 eV for the  $j=3/2$  peak and 0.42 eV for the  $j=1/2$  peak (see Table 1).

In contrast, the Mn core-level spectra show broader peaks with satellites. Figure 1(b) shows the Mn 2p spectrum split by the spin-orbital interaction. The

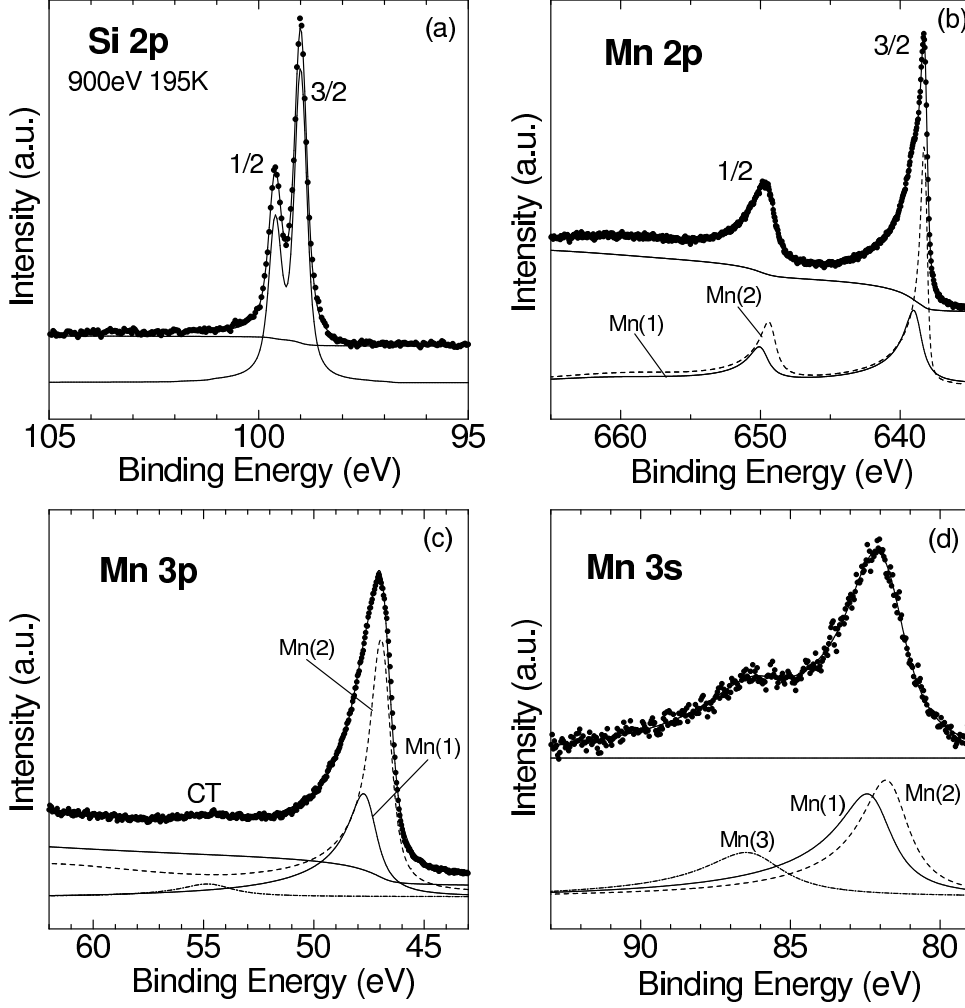


Fig. 1. Core-level photoemission spectra of  $\text{Mn}_5\text{Si}_3$  measured at 195 K for  $h\nu=900$  eV; (a) Si 2p, (b) Mn 2p, (c) Mn 3p, and (d) Mn 3s states. Dots are the raw data and the solid curves through them are the results of fittings. The other curves are the respective components and the secondary electron background for the fittings.

peaks at  $E_B=638$  eV and 650 eV correspond to the  $j=3/2$  and  $j=1/2$  states. The  $j=3/2$  peak cannot be explained by a single asymmetric component. It seems to be composed of a weaker peak at higher  $E_B$  and a stronger peak at lower  $E_B$ . Therefore, both  $j=3/2$  and  $1/2$  peaks are deconvoluted into two components as labeled by Mn(1) and Mn(2). The asymmetry parameter  $\alpha$  for the Mn(2) component is evaluated to be slightly smaller than that for the Mn(1) component as shown in Table 1. The intensity ratio of the Mn(1) and Mn(2) is roughly 2:3. The energy separation of them is 0.66 eV. The values of FWHM of the Mn 2p spectrum are roughly three times larger than that of Si 2p spectrum except for the Mn(2) component in the  $j=3/2$  peak of the Mn 2p spectrum.

Next, we show the Mn 3p spectrum in Fig. 1(c). A single prominent peak

is observed at  $E_B=47$  eV. Due to the 3p-3d multiplet effect, the spin-orbit splitting is not directly observed. There appears a small hump near  $E_B=55$  eV in addition to the main peak. This hump may correspond to the charge-transfer (CT) satellite of the main peak. It is not clearly recognized in other Mn core-level spectra because of its smallness. The smallness of this CT satellite intensity implies the dominance of the  $d^{n+1}\underline{L}$  final state for the main peak. Namely, the 3p core hole is well screened by the ligand electron. This is consistent with the good electric conductivity of this compound [1,5]. The main peak at  $E_B=47$  eV can not be fit by a single asymmetric Lorentzian but still be deconvoluted into two components of Mn(1) and Mn(2) with small and large intensities separated by the binding energy of 0.98 eV (see Table 1). The asymmetry  $\alpha$  of Mn(1) component is higher than that of Mn(2). The intensity ratio of them is again roughly estimated as 2:3. All the values of FWHM in the Mn 3p components are three to five times larger than that of the Si 2p components.

In Fig. 1(d) is shown the Mn 3s photoemission spectrum. There are two broad peaks separated by  $\sim 4$  eV. At first, the larger peak was tentatively deconvoluted into two components of Mn(1) and Mn(2) with the intensity ratio of 2:3 as in the case of Mn 2p and 3p spectra, where the FWHM was also larger for the Mn(1) component. The smaller peak at  $E_B \sim 86.5$  eV can be mostly attributed to the spin-exchange interaction. In 3d transition metal compounds, a well separated satellite by spin-exchange interaction can only be seen for the 3s orbital. This is because the multiplet effect in the 3s spectrum is less prominent than in the other core-level spectra and the magnitude of the exchange integral between the 3d and each core-level is the largest for the 3s level [14,15,16]. Then, we also deconvoluted this small peak into two components corresponding to the Mn(1) and Mn(2) components by assuming a relative intensity of 2:3. Then, the intensities of both components in the small peak were evaluated to be only  $\sim 26\%$  of the sum of the Mn(1) and Mn(2) components in the main peak.

Judging from the energy separation of  $\sim 4$  eV between the main peak and this satellite peak, the  $S=3/2$  spin state with the  $d^3$  ( $Mn^{4+}$ ) states are empirically conceived for the Mn 3d spin state [17]. Corresponding to the degeneracy of this spin state, the intensity ratio of the spin-exchange satellite compared to the main peak is known as  $(2S)/(2S+2)$  in the atomic model. According to this simplest model, the intensity ratio of the satellite will be  $3/5=60\%$  of the main peak for the case of  $S=3/2$  spin state. For larger momentum value such as  $S=2$  ( $d^4$ ,  $Mn^{3+}$ ) or  $S=5/2$  ( $d^5$ ,  $Mn^{2+}$ ) in the high spin state, the ratio will become larger. The experimentally derived ratio of 26 % is much smaller than these values. Thus, further consideration is required to interpret the observed results.

From the neutron diffraction measurements, several different spin alignments

are proposed for the lower temperature antiferromagnetic phases [8,9,10,11,12]. Some of them predict complex magnetic structures with non-equivalent electronic states in the  $\text{Mn}_{II}$  6(g) site [8,9,11]. In most cases, smaller magnetic moments are predicted for the  $\text{Mn}_I$  4(d) site (as summarized in Ref. 12). Furthermore, the band calculation predicts that the crystallographic  $\text{Mn}_I$  4(d) site has rather itinerant 3d electrons and the  $\text{Mn}_{II}$  6(g) site has rather localized ones [1]. In the photoemission spectroscopy, spin-exchange interaction effect is commonly seen as a localized feature both above and below a magnetic transition temperature [14,15]. If we apply these electronic configurations such as itinerant and localized Mn 3d electrons to the present case at 195 K in the paramagnetic state, it is conceivable that the spin-exchange satellite will be mostly derived from the  $\text{Mn}_{II}$  6(g) site. Consequently, the Mn 3s spectrum can be deconvoluted into three components: namely the larger peak at  $E_B=82$  eV consists of the Mn(1) and Mn(2) components whereas the smaller satellite peak at  $E_B=86.5$  eV consists of one component, Mn(3). Then, the intensity of the satellite Mn(3) component comes close to  $3/5=60\%$  of the Mn(2) intensity in reasonable agreement with the prediction for the  $S=3/2$  state. Therefore, we come to the conclusion that the Mn(2) and Mn(3) components are the main and the satellite peaks split by the spin-exchange interaction. Although the Mn(1) component should also have the spin-exchange satellite, the energy separation between them will be small enough and the satellite structure may not be clearly recognizable because of the FWHM and  $\alpha$ . Eventually, the intensity of the Mn(1) comes to 68 % of the ‘total’ intensity of Mn(2)+Mn(3) in agreement with the ratio of Mn(1):Mn(2) $\sim$ 2:3 as in the case of the Mn 2p and 3p spectra.

Table 1 summarizes the fitting parameters for each spectrum; binding energy, energy difference between the Mn(1) and Mn(2), asymmetry parameter  $\alpha$ , intensity ratio of Mn(1)/Mn(2), and the experimental full width at half maximum (FWHM). Larger FWHM and  $\alpha$  are seen for all the Mn(1) components compared with the Mn(2) components. The peak asymmetry  $\alpha$  is related to the infrared divergence or the high density of states (DOS) of the Mn 3d states near the Fermi level. The common tendency of higher  $\alpha$  of the Mn(1) component seen for all 2p, 3p and 3s spectra suggests the higher Mn 3d DOS near  $E_F$  on the Mn(1) site. We further note that all  $\alpha$  of the Mn core level spectra are more than ten times larger than that of the Si 2p state. This suggests that even the Mn(2) sites have some *itinerancy* compared to the Si site. The intensity ratios of Mn(1)/Mn(2), especially Mn(1)/{Mn(2)+Mn(3)} in the case of Mn 3s, are estimated as 0.63 $\sim$ 0.68. These values are very consistent with the site occupancy ratio of 2/3 between the  $\text{Mn}_I$  4(d) and  $\text{Mn}_{II}$  6(g) sites. Together with the discussion of the Mn 3s spin-exchange satellite, we conclude that the Mn(1) and Mn(2) components in the photoemission spectra are associated with the electronic states in the crystallographic  $\text{Mn}_I$  4(d) and  $\text{Mn}_{II}$  6(g) sites, respectively. In the Curie-Weiss type paramagnetic phase of  $\text{Mn}_5\text{Si}_3$  with metallic conduction above 99 K, it is experimentally revealed that the

spin is still large on the  $Mn_{II}$  6(g) site, whereas the magnitude of the spin is marginal on the  $Mn_I$  4(d) site.

orbital	$E_B$ (eV)	$\Delta E_B$ (1)-(2) (eV)	$\alpha$	Intensity ratio (1)/(2)	FWHM(eV)	
					j=3/2	j=1/2
Si 2p	99.00	-	0.02	-	0.43	0.42
Mn 2p	(1) 638.89	0.66	0.38	0.66	1.26	1.63
	(2) 638.23		0.31		0.59	1.32
Mn 3p	(1) 47.86	0.98	0.33	0.63	1.77	2.23
	(2) 46.88		0.26		1.16	1.21
Mn 3s	(1) 82.17	0.53	0.36	(1)/{(2)+(3)}	2.00	
	(2) 81.64		0.25	0.68	1.95	
	(3) 86.19	(3)-(2)	0.28	(3)/(2)	3.03	
	4.55	0.58				

Table 1

Fitting parameters used for the deconvolution of the inner core spectra; binding energies, energy shifts, asymmetry parameter  $\alpha$ , intensity ratios of Mn(1)/Mn(2), and experimental full width at half maximum (FWHM). For the Mn 3s spectrum are given the energy shifts of Mn(3) from Mn(2) components and the intensity ratios of Mn(1)/{Mn(2)+Mn(3)} and Mn(3)/Mn(2).

Figure 2 shows the valence band spectrum measured at  $h\nu=900$  eV. A secondary electron background is subtracted from the experimental spectrum in the figure. Three peak structures are recognized in the experimental spectrum up to  $E_B=7$  eV. The cross section of the Si 2p states is ten times smaller than that of the Mn 3d states at 900 eV [18]. Therefore, the photoemission features in the region of  $E_B=3.0$  eV $\sim E_F$  are mostly derived from the Mn 3d states. In addition, the measurement at this  $h\nu$  is rather bulk-sensitive compared with the lower  $h\nu$  photoemission [19,20]. The present spectrum is therefore reflecting the DOS of bulk Mn 3d states.

The total DOS predicted by the band calculation by L. Vinokurova et al. is shown by the thin solid curve in the lower panel [1]. For comparison, the thick solid curve shows its tentatively broaden spectrum with considering the Lorentzian FWHM of 200 meV, the experimental energy resolution of 100 meV, and the Fermi-Dirac function at 195 K. In the experimental spectrum, one observes a sharp peak near the Fermi level and broader peaks at the binding energies of 1.3 and 3.0 eV. They correspond roughly to the peaks of DOS of the band calculation as connected by arrows. The observed hump near 10 eV corresponds to the DOS of the Si 3s state which is commonly seen in photoemission spectra of 3d transition metal silicides [21]. In this way, the valence band bulk photoemission spectrum of  $Mn_5Si_3$  agrees qualitatively with

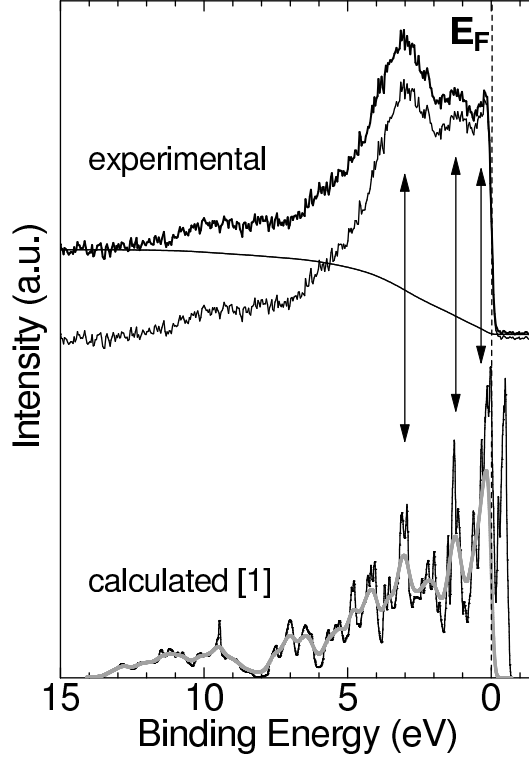


Fig. 2. High-resolution photoemission spectrum of valence band at 195 K for  $h\nu=900$  eV compared with the band calculation for the paramagnetic state of  $\text{Mn}_5\text{Si}_3$  done by L. Vinokurova et al. [1]

the result of the band calculation.

## 4 Conclusion

We have performed the bulk-sensitive high-resolution photoemission measurements on a single-crystal  $\text{Mn}_5\text{Si}_3$  by using synchrotron radiation. Each Mn core-level spectrum is found to consist of two components associated with crystallographic sites of  $\text{Mn}_I$  4(d) and  $\text{Mn}_{II}$  6(g). The large asymmetry  $\alpha$  of the photoemission spectra of the Mn core states indicates that the DOS near the Fermi energy consists mostly of the Mn 3d electron states. The valence band spectrum corresponds well to the DOS of the bulk electronic states.

## 5 Acknowledgements

We are grateful to Dr. T. Muro and Dr. Y. Saitoh for their assistance as beam line scientists. The research was performed at SPring-8 under the support of a

Grant-in-Aid for the COE Research (10CE2004) of the Ministry of Education, Culture, Sports, Science, and Technology (MEXT), Japan.

## References

- [1] L. Vinokurova, V. Ivanov, E. Kulatov and A. Vlasov, *J. Magn. Magn. Mat.* 90,91 (1990) 121.
- [2] H.J. Al-Kanani, J.G. Booth, *J. Magn. Magn. Mat.* 140-144 (1995) 1539.
- [3] L. Vinokurova, V. Ivanov, E. Kulatov, *Physica B* 211 (1995) 96.
- [4] M. E. Sheinker, R. P. Krentsis, P. V. Gel'd, *Sov. Phys. Solid State* 19 (1977) 1109.
- [5] R. Haug, G. Kappel, A. Jaegle, *J. Phys. Chem. Solids* 41 (1980) 539.
- [6] B. Aronsson, *Acta Chem. Scand.* 14 (1960) 1414.
- [7] K. Amark, B. Boren, A. Westgren, *Sv. Kem. Tidsk.* 48 (1936) 273.
- [8] P. J. Brown, J. B. Forsyth, V. Nunez, F. Tasset, *J. Phys. Condens. Matter* 4 (1992) 10025.
- [9] P. J. Brown, J. B. Forsyth, *J. Phys. Condens. Matter* 7 (1995) 7619.
- [10] A. Z. Menshikov, A. P. Vokhmyanin, Yu. A. Dorofeev, *Phys. Stat. Sol.* 158 (1990) 319.
- [11] G. H. Lander, P. J. Brown, J. B. Forsyth, *Proc. Phys. Soc.* 91 (1967) 332.
- [12] A. Z. Menshikov, A. M. Balagurov, A. I. Beskrovney, A. P. Vokhmyanin, and D. M. Morozov, *Matt. Sci. Forum* 321-324 (2000) 659.
- [13] S. Doniach and M. Sunjic, *J. Phys. C* 3 (1970) 285.
- [14] C. S. Fadley, D. A. Shirley, A. J. Freeman, P. S. Bagus and J. V. Mallow, *Phys. Rev. Lett.* 23 (1969) 1397.
- [15] C. S. Fadley and D. A. Shirley, *Phys. Rev. A* 2 (1970) 1109.
- [16] F. Parmigiani and L. Sangaletti, *J. Electr. Spectr. Rel. Phen.* 98-99 (1999) 287.
- [17] J. C. Carver, G. K. Schweitzer and T. A. Carlson, *J. Chem. Phys.* 57 (1972) 973.
- [18] J. J. Yeh and I. Lindau, *Atomic Data and Nuclear Data Tables* 32 (1985) 1-155.
- [19] A. Sekiyama, T. Iwasaki, K. Matsuda, Y. Saitoh, Y. Onuki and S. Suga, *Nature* 403 (2000) 396.
- [20] S. Suga and A. Sekiyama, *J. Electron Spectrosc. Rel. Phenom.* 114-116 (2001) 659.

- [21] W. Speier, E. v. Leuken, J. C. Fuggle, D. D. Sarma, L. Kumar, B. Dauth, K. H. J. Buschow, *Phys. Rev. B* 39 (1989) 6008.